ENERGY DISTRIBUTION IN GLARE AND 2024-T3 ALUMINIUM DURING LOW-VELOCITY IMPACT

F.D. Morinière, R.C. Alderliesten, R. Benedictus
Structural Integrity Group, Faculty of Aerospace Engineering, Delft University of Technology, Kluyverweg 1, 2629 HS Delft, The Netherlands
F.D.Moriniere@tudelft.nl;R.C.Alderliesten@tudelft.nl;R.Benedictus@tudeflt.nl

Keywords: *impact, GLARE FML, aluminium, energy, delamination*

Abstract

This paper presents a theoretical and experimental comparative study on the low-velocity impact behaviour of GLARE Fibre-Metal Laminate (FML). Using the Classical Laminate Theory and the First-order Shear Deformation Theory, an analytical model was developed to predict the impact behaviour of FMLs. Delamination onset and contact increase during perforation were taken into account. New generic expressions were derived for strain energy and contact force. Absorbed energy, impact force, maximum deflection and impact velocity were predicted within 5% of test results. GLARE 5-2/1-0.4 is 72% more resistant than its monolithic 2024-T3 aluminium counterpart of the same thickness.
Because GLARE is made of thin high strength layers that can undergo large deformation, this hybrid material is an ideal candidate for impact prone structures. This general understanding will support the development of high-energy absorbing FML concepts.

1 Introduction

Fibre-Metal Laminates (FMLs) are lightweight hybrid composite materials that consist of alternating aluminium layers bonded to fibre-reinforced epoxy layers. GLARE (GLAss-Reinforced) FML demonstrates outstanding damage tolerance capabilities [1] in combination with excellent impact resistance when compared to composites and metals [2]. With such a high structural efficiency, designers gained interest in the application of GLARE in aircraft structures. Originally developed for primary structures such as fuselage and wing skins, this material is also applied in cargo floors, engine cowlings, patch repair, stringers, cargo containers and seamless tubes [3-5].

Impact is a type of damage that has to be considered in the design process for safety reasons [6]. However, no available method can predict the perforation behaviour of FMLs under impact loading. Multiple studies have resulted in the theoretical prediction of the impact response of GLARE under various loading conditions [7-12] but the methodologies focused mainly on the elastic response which represents a minor portion of the perforation response. Consequently, the impact strength substantiation is typically evaluated via testing. This method is time consuming and because of scatter in the results, it requires a large amount of coupons. The development of impact resistant concepts is therefore limited. A new technique is necessary to assess the impact performance of FMLs.

In this paper, a theoretical model will be presented to predict the perforation behaviour of GLARE under low-velocity impact. The Classical Laminate Theory (CLT) will be used with the First-order Shear Deformation Theory (FSDT) to perform a sequential failure analysis. This new method will introduce new equations for strain energy and impact force. Besides, it will be able to evaluate the contribution of the material constituents of GLARE 5-2/1-0.4. The present approach which provides a general understanding of the impact behaviour of FMLs is not found in the literature.

2 Experimental Arrangement

Panels of GLARE 5-2/1-0.4 were prepared by hand lay-up technique. This laminate consists of a [0°/90°/90°/0°] composite core of S2-glass/FM94-epoxy prepregs embedded in two layers of 2024-T3 aluminium of 0.4 mm. Plates of the same aluminium alloy were used as a reference. Both materials had a thickness of 1.3 mm. Mechanical properties were taken from [13-15]. For modelling purposes, aluminium is isotropic. The Young's modulus is then the average between the available data. According to ASTM E8M [16], 12 dogbone samples of 0.4mm-thick 2024-T3 aluminium – 6 in the rolling direction and 6 in the transverse one – were tested to estimate the modulus of plasticity. Thereby, a bilinear stress-strain curve was assumed for aluminium with a mean Young's modulus of 70.15 GPa and a mean modulus of plasticity of 1.60 GPa.

A series of impact tests were executed at room temperature at the centre of rectangular plates. The rolling direction and the 0° fibre orientation corresponded to the major axis of the rectangle. The 150 mm x 100 mm flat panels were fully clamped in a fixture with a 125 mm x 75 mm aperture. A falling weight of 1.075 kg hit the specimens via a conical-shaped steel impactor with a hemispherical nose whose radius was 6.35 mm. The exact dimensions are stated in ASTM D5628 [17]. Four panels were used for each material to determine the perforation threshold. Perforation occurred when cracking in aluminium was observed on both sides of the specimens.

3 Model Development

3.1 Approach

The impact response type is governed by the impactor–plate mass ratio and not by impact velocity [18]. If the impactor mass divided by the effective mass of panel is lower than 1/5 (dynamic wave-controlled impact), the plate deformation is localised to the vicinity of the impact point and, the contact force and plate deformation are never in phase. If the impactor-total plate mass ratio is larger than 2 (quasi-static boundary-controlled impact), the entire plate is deformed during the impact, and the contact force and plate deformation are slightly out of phase, as shown in Fig. 1.

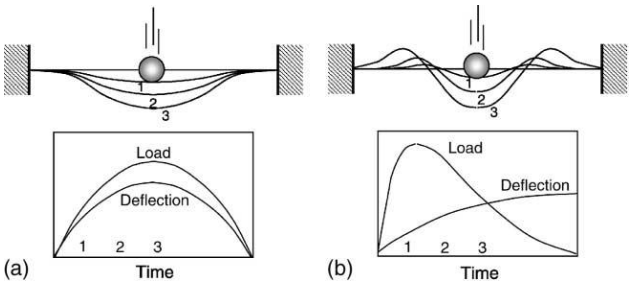

Fig. 1. a) Quasi-static and b) dynamic impact responses [19]

In this study, the impactor-plate mass ratio was larger than 31. A quasi-static analysis can be realised to compute stresses until detection of failure though the strain rate affects mechanical properties of 2024-T3 aluminium and S2-glass fibres [2, 20, 21].

Considering that the full plate participates in the response, the strain rate is approximated by dividing the impact velocity by the average-half of the plate dimensions.

The empirical Johnson-Cook model accounts for strain rate effect on the yield strength of aluminium [22]. Thermal effect is ignored as tests were operated at room temperature. This model appraises also failure strain. The value applied in this research is the average between the strain obtained with the original method and the strain found with an updated version [23]. Furthermore, the effect of plate thickness is not included in the Johnson-Cook approach. As ductility can decrease up to 6% for a thickness of 3 cm [9, 24], a 12% failure strain is used for a 1.3mm-thick plate.

Regarding glass composites, a strain rate of 100 s^{-1} results in a 10% increase in strength from static values [9, 25].

Hereby, the established method will define for an initial strain rate the evolution of the energy partition between the material constituents until the perforation limit.

Deformation, delamination, fracture and petaling are selected among several failure modes [2] to form the total absorbed energy:

$$E_{abs\ tot} = E_{def} + E_{del} + E_{frac} + E_{petal} \quad (1)$$

At perforation threshold this total energy equals the kinetic energy of impact. The impact velocity limit (V_0) is given by:

$$V_0 = \sqrt{\frac{2E_{abs\ tot}}{M}} \quad (2)$$

with (M) the mass of projectile. In order to calculate the total absorbed energy during impact, the substance of each component in Eq. (1) has to be quantified.

3.2 Energy Absorbed in Global Flexure

An initial in-plane radius of 1.588 mm was determined experimentally to account for the increase of the radial contact. The corresponding initial dent depth defines an initial arc length which represents the true contact radius (r). When a layer fails, the penetration depth increases with the thickness of the failed layer, which leads to a larger arc length. This simplification in the penetration of a hemispherical nose into a laminate is valid if the laminate thickness does not exceed a height equivalent to the nose radius.

Since large deflection is expected, the in-plane displacements are neglected. The deflection profile (w) of the neutral line of the laminate is a revised formulation of a FE analysis [10]:

$$w(x,y) = \begin{cases} \Delta & 0 \le x \le r \\ & 0 \le y \le r \\ w_0\left(1-\frac{2x}{a}\right)^2\left(1-\frac{2y}{b}\right)^2 & r \le x \le a/2 \\ & r \le y \le b/2 \end{cases} \quad (3)$$

$$with \quad w_0 = \Delta \Big/ \left[\left(1-2r/a\right)^2\left(1-2r/b\right)^2\right] = \Delta/c$$

This shape meets the boundary conditions of a fully clamped plate with maximum displacement (Δ) at the centre.

In the FSDT [26], Von-Kármán strains represent membrane deformation and bending strains are calculated from the neutral axis of the plate. The corresponding off-axis stresses in the CLT [26] are computed in each layer at the height where they are maximum. As soon as an aluminium layer yields, the Young's modulus is updated with the strain-hardened modulus of plasticity. When a composite ply fails, the stresses in the principal axes of the failed layer are distributed into the intact ones according to their respective stiffnesses. Then, a failed layer has zero stiffness for the same thickness.

For small deformation, stresses are limited by the Von-Mises criterion for aluminium and by the Tsai-Hill criterion for unidirectional composite to obtain the maximum allowed deflection at each failure step until the last fibre layer breaks. Then, the damage process ends with the Johnson-Cook failure strain as aluminium layers undergo large deformation. Unlike for the thick aluminium, elastic springback is considered in GLARE. Permanent deflection equals the difference between the maximum deflection and the displacement when first failure occurs.

Taking into account the assumptions of the CLT and integrating strain energy along the laminate thickness, membrane energy (U_m), flexural-extensional coupling energy (U_c) and bending energy (U_b) are gathered:

$$U_m = \frac{w_0^4}{a^8 b^8}\left[A_{11}\frac{32}{45}\alpha^5\beta^9 + \left(2A_{12}+4A_{66}\right)\frac{32}{49}\alpha^7\beta^7 + A_{22}\frac{32}{45}\alpha^9\beta^5 + \frac{8}{3}\left(A_{16}\alpha^6\beta^8 + A_{26}\alpha^8\beta^6\right)\right] = w_0^4 K_m$$

$$U_c = -\frac{w_0^3}{a^6 b^6}\left[B_{11}\frac{32}{21}\alpha^3\beta^7 + \left(2B_{12}+8B_{66}\right)\frac{64}{25}\alpha^5\beta^5 + B_{22}\frac{32}{21}\alpha^7\beta^3 + 16\left(B_{16}\alpha^4\beta^6 + B_{26}\alpha^6\beta^4\right)\right] = w_0^3 K_c \quad (4)$$

$$U_b = \frac{w_0^2}{a^4 b^4}\left[D_{11}\frac{32}{5}\alpha\beta^5 + \left(D_{12}+8D_{66}\right)\frac{64}{9}\alpha^3\beta^3 + D_{22}\frac{32}{5}\alpha^5\beta + 32\left(D_{16}\alpha^2\beta^4 + D_{26}\alpha^4\beta^2\right)\right] = w_0^2 K_b$$

$$with \quad \alpha = a - 2r \quad and \quad \beta = b - 2r$$

Strain energy absorbed at a step *i* gives:

$$U_i = \left(w_{0_i}^4 - w_{0_{i-1}}^4\right)K_{m_i} + \left(w_{0_i}^3 - w_{0_{i-1}}^3\right)K_{c_i} + \left(w_{0_i}^2 - w_{0_{i-1}}^2\right)K_{b_i} \quad (5)$$

Hence, the total absorbed strain energy (E_{def}) becomes:

$$E_{def} = \sum U_i \quad (6)$$

The impact load (F) can be derived from Eq. (4). With the external work (W_{ext}) done by this force, the total potential energy (Π) yields:

$$\Pi = W_{\text{int}} - W_{ext} = U_m + U_c + U_b - F\Delta \quad (7)$$

When minimizing with respect to Δ, the indentation load at each failure event is:

$$F = 4\frac{\Delta^3}{c^4}K_m + 3\frac{\Delta^2}{c^3}K_c + 2\frac{\Delta}{c^2}K_b \quad (8)$$

3.3 Energy Absorbed in Delamination

Assuming a greatly simplified shear stress distribution, delamination will propagate in mode II at a critical force [27]:

$$F_{del}^2 = \frac{8\pi^2 E_{lam} t_{lam}^3 G_{IIc}}{9\left(1-\nu_{lam}^2\right)} \quad (9)$$

where (E_{lam}) is the plate stiffness, (t_{lam}) the thickness and (ν_{lam}) the Poisson's ratio. (G_{IIc}) is the mode II critical interlaminar shear fracture toughness of the prepreg. Delamination grows in the plate's mid-plane as the interlaminar shear strength (*ILSS*) of the composite layer is exceeded [28]. Thereupon, the energy due to delamination (E_{del}) equals:

$$E_{del} = \frac{2\pi t_{lam} E_{lam} G_{IIc}^2}{9\left(1-\nu_{lam}^2\right) ILSS^2} \quad (10)$$

If the force induced by plate deformation at a given step is lower than the load required for the onset of delamination, delamination energy is ignored.

3.4 Energy Absorbed in Tensile Fracture

The tensile fracture energy (E_{frac}) of *n* layers of a thickness (t) is the product of the energy density to tensile failure (e_t) by the volume of the dent produced after impact:

$$E_{frac} = ne_t\pi r^2 t \quad (11)$$

3.5 Energy Absorbed in Petaling

As the projectile pierces through aluminium, it bends back material around its periphery. At the end of the failure process the plastic work in petaling (E_{petal}) of *n* layers is:

$$E_{petal} = n2\pi r\sigma_0 t^2\theta \quad (12)$$

with (σ_0) the yield strength of aluminium and (θ) the angle of petaling.

4 Results

Damage in the perforated specimens can be observed in Fig. 2.

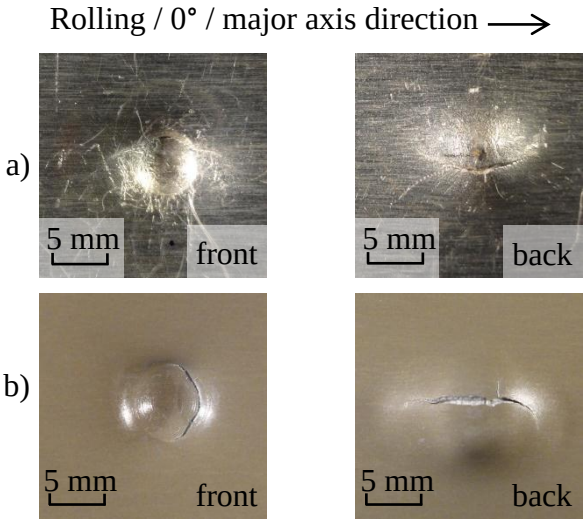

Fig. 2. Aluminium cracking in a) AL 2024-T3 and b) GLARE 5-2/1-0.4

The impact characteristics that emanate from the described model are compared with recorded data in Table 1 and Table 2.

Table 1. Characteristics of 2024-T3 aluminium

t = 1.3 mm – ρ_{areal} = 3.61 kg/m^2			
	Model	Test	% diff.
F_{max} [kN]	3.19	3.34	-4.36%
Δ_{max} [mm]	8.72	8.64	0.98%
V_0 [m/s]	4.49	4.56	-1.54%
E_{def} [J]	8.78	-	-
E_{petal} [J]	1.53	-	-
E_{frac} [J]	0.52	-	-
$E_{abs\ tot}$ [J]	10.83	11.15	-2.83%
E_s [Jm^2/kg]	3.00	3.09	-2.83%

Table 2. Characteristics of GLARE 5-2/1-0.4

t = 1.3 mm – ρ_{areal} = 3.20 kg/m^2			
	Model	Test	% diff.
F_{max} [kN]	4.05	4.01	1.02%
Δ_{max} [mm]	11.58	11.60	-0.21%
V_0 [m/s]	5.79	5.95	-2.72%
E_{def} [J]	14.72	-	-
E_{petal} [J]	0.94	-	-
$E_{frac\ AL}$ [J]	1.89	-	-
E_{del} [J]	0.14	-	-
$E_{frac\ GE}$ [J]	0.31	-	-
$E_{abs\ tot}$ [J]	18.01	16.99	5.99%
E_s [Jm^2/kg]	5.63	5.31	5.99%

Predictions are in good agreement with test results. In general, precision amounts to 1.6% for total absorbed energy ($E_{abs\ tot}$) and 2% for impact velocity (V_0). Maximum deflection (Δ_{max}) is determined with an accuracy of 0.4% while it rises to 1.7% for impact force (F_{max}). The analysis demonstrates that the studied plates are impact resistant structures given that impact energy is absorbed via plate deformation at 82% in GLARE 5-2/1-0.4 and 81% in 2024-T3 aluminium. In contrast with this aspect the specific absorbed energy (E_s) reveals the true structural efficiency of the constructions. Test results specify that GLARE is 72% more resistant than its plain aluminium counterpart of equivalent thickness.

Besides these impact characteristics, the low-velocity impact behaviour of GLARE 5-2/1-0.4 and 2024-T3 aluminium can be evaluated with the evolution of force and energy with respect to displacement as shown in Fig. 3 and Fig. 4. The predicted energy-displacement (*E*-*D*) curves fit well with test data. Given that force derives from energy, modelling discrepancies are magnified in the force-displacement (F-*D*) curves.

Three small peaks can be noticed in the beginning of the predicted *F*-*D* curve of GLARE. In the model failure is detected with Von Mises and Tsai-Hill criteria. These principles detect rupture for a complete layer which is not likely to happen in reality as much as the assumption for which a failed layer has zero stiffness for the same thickness. However, this estimate has to be interpreted such that a failed layer at the impact location will no longer carry load in the plate. This hypothesis creates little peak loads that are not recorded during testing. The first two ones designate aluminium yielding – non-impacted aluminium followed by impacted aluminium layer – and the last one, for the last fibre layer to rupture. The maximum load characterises the failure of the back aluminium layer. The slope towards this maximum value is predicted at a force 0.5 kN less than test data.

The theoretical *F*-*D* curve of plain aluminium pictures the previously observed patterns and therefore suggests improvements for the construction of the method. The first peak represents aluminium yielding. This value is more important given that the thickness of aluminium is 3.25 times higher than a single aluminium layer in GLARE. The ramp towards maximum force is about 1 kN less for a given recorded displacement. Based on these remarks, the modelled stiffness estimated for aluminium is too conservative. Subsequently, it will be reconsidered with the Ramberg-Osgood model or a rigid plastic assumption.

From this preliminary analysis, aluminium is dominating the global impact behaviour of

GLARE. The predicted absorbed energy-displacement curves fit well with test data. A deeper examination into the energy partition in the laminate will give further details on the role of the material constituents.

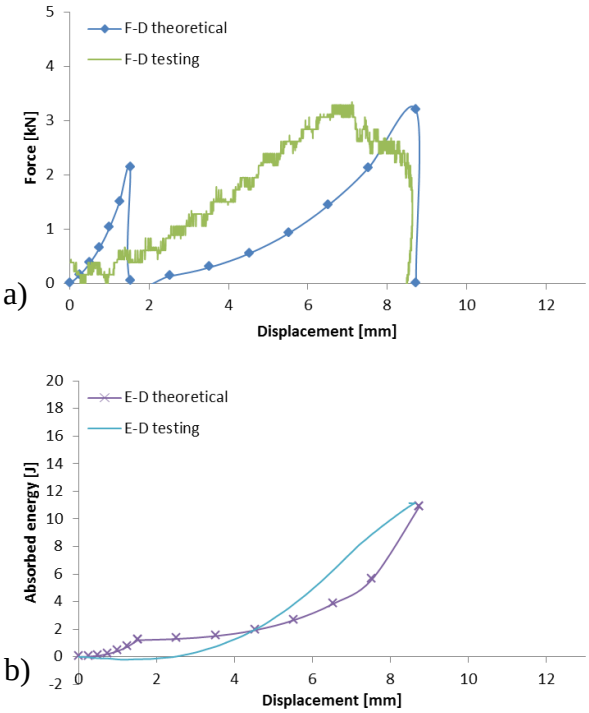

Fig. 3. a) F-D and b) E-D curves of 2024-T3 aluminium

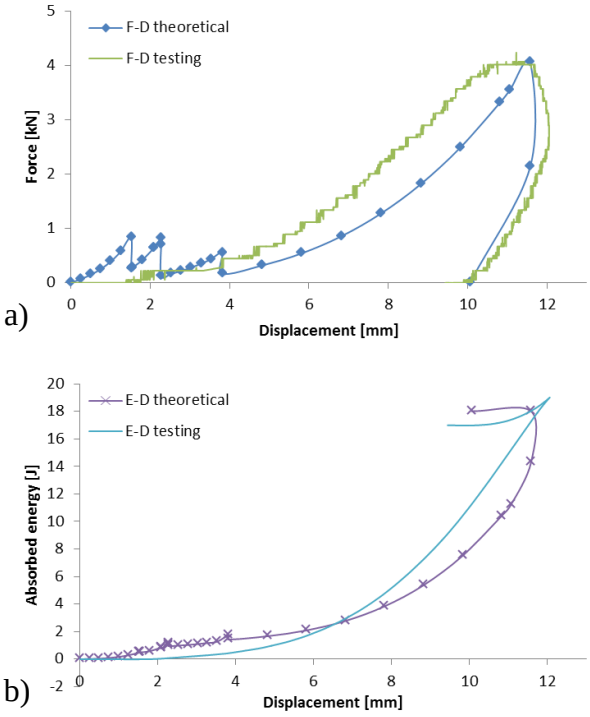

Fig. 4. a) F-D and b) E-D curves of GLARE 5-2/1-0.4

5 Discussion

5.1 Global Strain Energy

In the developed methodology the energy absorbed by the plate is the summation of strain energy and energy due to failure modes as summarised in Table 3. Strain energy is decomposed into membrane (E_m), tensional-flexural coupling (E_c) and bending (E_b) energies. Energy of failure modes (E_{fail}) is partitioned into delamination, fracture and petaling. In GLARE the large majority of impact energy is absorbed at 77% via membrane deformation while bending energy accounts for 5% and coupling energy is negligible. In aluminium the proportion of membrane energy is still dominant (53%) with a relatively important contribution of coupling (17%) and bending (10%) energies.

Table 3. Absorbed energy partition

Energy	2024-T3	GLARE 5-2/1-0.4
E_m [J]	5.78 (53.34%)	13.93 (77.35%)
E_c [J]	1.90 (17.53%)	-0.02 (-0.13%)
E_b [J]	1.10 (10.18%)	0.82 (4.55%)
E_{fail} [J]	2.05 (18.95%)	3.28 (18.23%)
$E_{abs\ tot}$ [J]	10.83 (100.00%)	18.01 (100.00%)

As GLARE withstands a predicted displacement 33% larger than aluminium, GLARE can take advantage of its high membrane stiffness component. Indeed, membrane energy is proportional to displacement to the power 4, as seen in Eq. (5). Therefore, a laminate of thin high-strength layers that can endure large deformation will absorb more impact energy than a thick plate with high bending stiffness.

Strain energy evolution depicted in Fig. 5 supports this statement. When the 1.3mm aluminium deflects, the bending energy is higher than the membrane energy until 56% of maximum displacement and until 49% for coupling. On the contrary, the bending energy in

GLARE is greater than the membrane energy until 17% of maximum displacement and until 5% for coupling.

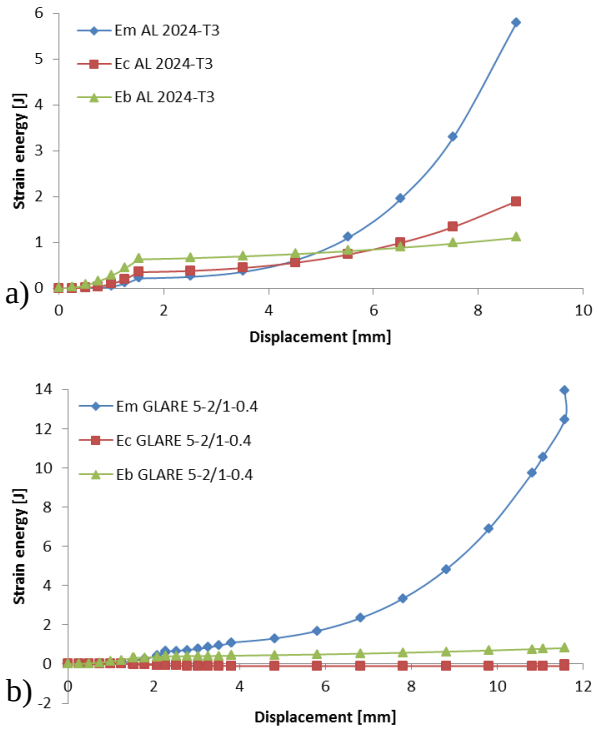

Fig. 5. Strain energy – displacement curves of a) AL 2024-T3 and b) GLARE 5-2/1-0.4

A second reason for which efficient membrane deformation occurs in GLARE is the presence of delamination. It shows evidence of an effective in-plane redistribution of the short-transverse load into the laminate. According to the model delamination does not contribute in the energy absorption. Nevertheless, delamination is supposed to occur at different locations depending on the side of the plate (see Fig. 2). At the non-impacted side aluminium cracking takes place at the centre of the impact location while it happens in the periphery of the visible dent at the impacted side. These are the different positions where delamination is assumed to initiate. At these specific locations delamination will reduce plate stiffness locally and will allow the layers to act as a number of separate thin layers in membrane deformation. Thus, aluminium layers do no longer benefit from the association with glass fibres. The high concentrated stresses that they withstand in the vicinity will induce crack initiation. Delamination is not a favourable failure mode in FML as it precipitates failure of aluminium layers.

5.2 Strain Energy among the Constituents

To further evaluate the separate role of the constituents of GLARE, the energy distribution is given in Fig. 6. As demonstrated in Section 5.1, GLARE undergoes large deformation and takes advantage of its high membrane stiffness. Interestingly, the aluminium layers absorb 94% of impact energy: 46% for the impacted aluminium layer and 48% for the aluminium layer farther from the impacted side. The remaining 5% is due to composites.

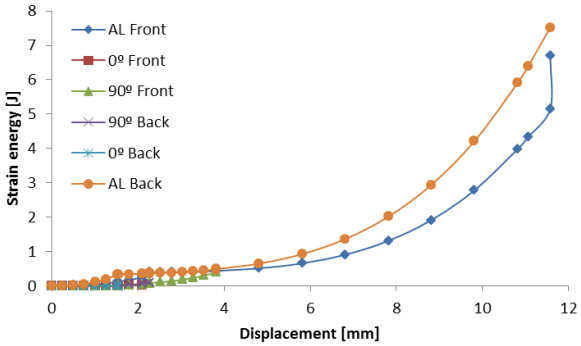

Fig. 6. Energy distribution among the constituents of GLARE 5-2/1-0.4

Fibres may absorb a minor part of impact energy but benefit the aluminium layers. Even if glass fibre layers break at small deflection their relatively high membrane stiffness attract load so that aluminium layers can withstand larger deformation safely. This advantage is depicted in Fig. 7.

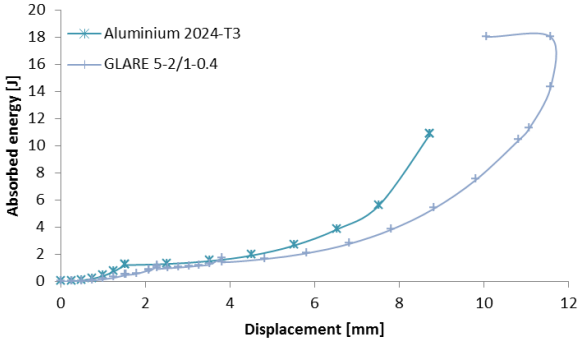

Fig. 7. Theoretical E-D curves

Based on the analysis, aluminium first cracking in GLARE 5-2/1-0.4 means that composite

layers are broken at the impact location. This element is of importance for impact resistance characterisation. In any case, Hagenbeek [2] indicated that the visible plastic zone surrounding the impact location always contains damage in the prepregs. Plastic areas are easy to detect and facilitate maintenance and repair.

6 Conclusion

A quasi-static analytical model has been developed to evaluate the perforation behaviour of GLARE 5-2/1-0.4 and its 2024-T3 aluminium counterpart under low-velocity impact. Using basic principles such as the First-order Shear Deformation Theory and the Classical Laminate Theory, it exhibits the function of the material constituents.

Absorbed energy, impact velocity, maximum deflection and impact force were within 5% of test results. Even if the aluminium and GLARE specimens are impact resistant – 80% of the impact energy is absorbed via plate deformation – GLARE has a structural efficiency 72% higher than monolithic aluminium. Indeed, glass fibres can withstand relatively large deformation and their high membrane stiffness attracts the impact load, which allows aluminium layers to flexure safer at larger deflection. An impact resistant fibre-metal laminate is the one containing high strength composites that can endure large deformation.

Further research will determine velocity and time evolution to generate the impact response. The extended tool will therefore help in impact damage assessment and it will support the development of impact resistant FML concepts.

Acknowledgements

This work was supported by NL Agency and GTM Advanced Products. The authors thank Dr. M. Sadighi from Amirkabir University of Technology for helpful discussion.

References

[1] Alderliesten RC and Homan JJ. Fatigue and damage tolerance issues of GLARE in aircraft structures. *International Journal of Fatigue*, Vol. 28, No. 10, pp 1116-1123, 2006.

[2] Vlot A and Gunnink JW. *Fibre metal laminates - an introduction.* Kluywer Academic Publisher, 2001.

[3] Gunnink JW et al. GLARE technology development 1997–2000. *Applied Composite Materials*, Vol. 9, No. 4, pp 201-219, 2002.

[4] Woerden HJM, Sinke J and Hooijmeijer PA. Maintenance of GLARE structures and GLARE as riveted or bonded repair material. *Applied Composite Materials*, Vol. 10, No. 4, pp 307-329, 2003.

[5] Vermeeren CAJR. An historic overview of the development of fibre metal laminates. *Applied Composite Materials*, Vol. 10, No. 4, pp 189-205, 2003.

[6] Vlot A. *Low-velocity impact loading on fibre reinforced aluminium laminates (ARALL and GLARE) and other aircraft sheet materials.* Delft University of Technology, Faculty of Aerospace Engineering, Report LR-718, 1993.

[7] Vlot A. Impact properties of fibre metal laminates. *Composites Engineering*, Vol. 3, No. 10, pp 911-927, 1993.

[8] Vlot A, Kroon E and La Rocca G. Impact response of fiber metal laminates. *Key Engineering Materials*, Vol. 141-143, pp 235-276, 1998.

[9] Hoo Fatt MS et al. Ballistic impact of GLARE fiber-metal laminates. *Composite Structures*, Vol. 61, No. 1-2, pp 73-88, 2003.

[10] Lin C and Hoo Fatt MS, Perforation of composite plates and sandwich panels under quasi-static and projectile loading. *Journal of Composite Materials*, Vol. 40, No. 20, pp 1801-1840, 2006.

[11] Payeganeh GH, Ashenai Ghasemi F and Malekzadeh K. Dynamic response of fiber–metal laminates (FMLs) subjected to low-velocity impact. *Thin-Walled Structures*, Vol. 48, No. 1, pp 62-70, 2010.

[12] Tsamasphyros GJ and Bikakis GS. Dynamic response of circular GLARE fiber-metal laminates subjected to low velocity impact. *Journal of Reinforced Plastics and Composites*, 2011.

[13] Iaccarino P, Langella A and Caprino G. A simplified model to predict the tensile and shear stress-strain behaviour of fibreglass/aluminium laminates. *Composites Science and Technology*, Vol. 67, No. 9, pp 1784-1793, 2007.

[14] O'Higgins RM, McCarthy MA and McCarthy CT. Comparison of open hole tension characteristics of high strength glass and carbon fibre-reinforced composite materials. *Composites Science and Technology*, Vol. 68, No. 13, pp 2770-2778, 2008.

[15] Zhang X et al. Fail-safe design of integral metallic aircraft structures reinforced by bonded crack retarders. *Engineering Fracture Mechanics*, Vol. 76, No. 1, pp 114-133, 2009.

[16] *ASTM E8M, Standard test methods fortTension testing of metallic materials [Metric]*. ASTM International, 2004.
[17] *ASTM D5628, Standard test method for impact resistance of flat, rigid plastic specimens by means of a falling dart (tup or falling mass).* ASTM International, 1996.
[18] Olsson R. Mass criterion for wave controlled impact response of composite plates. *Composites Part A: Applied Science and Manufacturing*, Vol. 31, No. 8, pp 879-887, 2000.
[19] Olsson R. Closed form prediction of peak load and delamination onset under small mass impact. *Composite Structures*, Vol. 59, No. 3, pp 341-349, 2003.
[20] Vlot A and Krull M. Impact damage resistance of various fibre metal laminates. *J. Phys. IV France*, Vol. 7, No. C3, pp C3-1045-C3-1050, 1997.
[21] De Vries TJ. *Blunt and sharp notch behaviour of GLARE laminates.* Delft University of Technology, Faculty of Aerospace Engineering, Doctoral Thesis, 2001.
[22] Lesuer DR. *Experimental investigations of material models for Ti-6Al-4V titanium and 2024-T3 aluminum.* U.S. Federal Aviation Administration, Office of Aviation Research, Report DOT/FAA/AR-00/25, 2000.
[23] Kay G. *Failure modeling of titanium 6Al-4V and aluminum 2024-T3 with the Johnson-Cook material model.* U. S. Federal Aviation Administration, Office of Aviation Research, Report DOT/FAA/AR-03/57, 2003.
[24] *MIL-HDBK-5H, Metallic materials and elements for aerospace vehicle structures.* MMPS-01, 1998.
[25] Armenakas A and Sciammarella C. Response of glass-fiber-reinforced epoxy specimens to high rates of tensile loading. *Experimental Mechanics*, Vol. 13, No. 10, pp 433-440, 1973.
[26] Berthelot JM. *Matériaux composites - comportement mécanique et analyse des structures.* 4e édition, TEC&DOC, 2005.
[27] Davies GAO, Hitchings D and Ankersen J. Predicting delamination and debonding in modern aerospace composite structures. *Composites Science and Technology*, Vol. 66, No. 6, pp 846-854, 2006.
[28] Sutherland LS and Guedes Soares C. Contact indentation of marine composites. *Composite Structures*, Vol. 70, No. 3, pp 287-294, 2005.

Copyright Statement